Environ. Sci. Technol. **2003**, *37,* 3701−3708

CO_2 Hydrate Composite for Ocean Carbon Sequestration

SANGYONG LEE,[†] LIYUAN LIANG,[†,‡] DAVID RIESTENBERG,[†] OLIVIA R. WEST,[†] COSTAS TSOURIS,*[,†] AND ERIC ADAMS[§]

Oak Ridge National Laboratory, P.O. Box 2008, Oak Ridge, Tennessee 37831-6181, Cardiff School of Engineering, University of Wales, Cardiff CF24 0YF, U.K., and Department of Civil and Environmental Engineering, Massachusetts Institute of Technology, 77 Massachusetts Avenue, Cambridge, Massachusetts 02139

Rapid CO_2 hydrate formation was investigated with the objective of producing a negatively buoyant CO_2−seawater mixture under high-pressure and low-temperature conditions, simulating direct CO_2 injection at intermediate ocean depths of 1.0−1.3 km. A coflow reactor was developed to maximize CO_2 hydrate production by injecting water droplets (e.g., ∼267 μm average diameter) from a capillary tube into liquid CO_2. The droplets were injected in the mixing zone of the reactor where CO_2 hydrate formed at the surface of the water droplets. The water-encased hydrate particles aggregated in the liquid CO_2, producing a paste-like composite containing CO_2 hydrate, liquid CO_2, and water phases. This composite was extruded into ambient water from the coflow reactor as a coherent cylindrical mass, approximately 6 mm in diameter, which broke into pieces 5−10 cm long. Both modeling and experiments demonstrated that conversion from liquid CO_2 to CO_2 hydrate increased with water flow rate, ambient pressure, and residence time and decreased with CO_2 flow rate. Increased mixing intensity, as expressed by the Reynolds number, enhanced the mass transfer and increased the conversion of liquid CO_2 into CO_2 hydrate. Using a plume model, we show that hydrate composite particles (for a CO_2 loading of 1000 kg/s and 0.25 hydrate conversion) will dissolve and sink through a total depth of 350 m. This suggests significantly better CO_2 dispersal and potentially reduced environmental impacts than would be possible by simply discharging positively buoyant liquid CO_2 droplets. Further studies are needed to address hydrate conversion efficiency, scale-up criteria, sequestration longevity, and impact on the ocean biota before in-situ production of sinking CO_2 hydrate composite can be applied to oceanic CO_2 storage and sequestration.

Introduction

Global emissions of CO_2 to the atmosphere have been predicted to increase from 7.4 billion t of carbon (Gt of C)/yr in 1997 to approximately 26 Gt of C/yr by 2100 (*1*). Marine carbon sequestration, which has been suggested as one method to counteract anthropogenic increases in atmospheric CO_2, takes advantage of the large CO_2 storage capacity (20 million Gt of C) offered by the world's oceans, in comparison with potential terrestrial (∼100 Gt of C) and geologic (300−3200 Gt of C) reservoirs (*2*−*4*). Proposed methods for direct injection of CO_2 to the ocean include rising CO_2 droplets released either from a bottom-mounted pipeline (*5*) or a moving ship (*6*), dense gravity currents formed from CO_2-enriched seawater (*7*), sinking large dry ice cubes (*8*), and deep CO_2 lakes (*9*).

Among these proposed options, formation of a rising droplet plume has been intensely studied because of its most advanced development and the relatively low cost (*10*−*12*). Recently, a class of options has been proposed that involves the release of CO_2-containing particles that are denser than seawater. These include the release of solid hydrate particles (*2, 3, 13, 14*), ice and hydrate-covered liquid CO_2 (*15*), and slurries of CO_2-enriched seawater containing solid $CaCO_3$ (*16*). The advantage of sinking CO_2 particles is that the CO_2 can reach deeper depths with high dispersion, thus increasing sequestration efficiency and minimizing environmental impacts (*1, 17*).

Pure CO_2 hydrate is denser than seawater and can be produced at high pressures (>4.5 MPa, equivalent to depths >0.45 km) and low temperatures (<10 °C), according to thermodynamic principles (*3, 4, 13*). Although CO_2 hydrate is expected to be unstable in seawater (*18*), the release of CO_2 in the ocean as sinking CO_2 hydrate particles, as opposed to rising liquid CO_2 droplets, could increase the residence time and prolong the storage of injected CO_2. Additionally, dissolution of CO_2 hydrate is slower than that of liquid CO_2 drops (*19*), which will facilitate greater dispersal of CO_2 in seawater and minimize the environmental impact. Producing droplets composed of mostly CO_2 hydrate by directly injecting liquid CO_2 into seawater will be very difficult to achieve (*20*). Laboratory experiments have demonstrated the production of CO_2 hydrate particles in a batch reactor at pressures corresponding to ocean depths of 450−500 m (*21*). The rapid formation of CO_2 hydrate requires vigorous agitation in the crystallization process, demanding an energy input that can be as high as 7% of a 100-MW power plant (*21*).

This paper investigates the formation of a sinking CO_2 hydrate mixture as an alternative to pure CO_2 hydrate. This mixture takes the form of a paste-like composite, which contains liquid CO_2, CO_2 hydrate, and water (referred to in this paper as "hydrate composite" or simply "composite"). Results of experiments using a coflow reactor are reported in which water was injected into liquid CO_2, forming a CO_2 hydrate composite before injection into the surrounding water. The effects of pressure and flow rates of water and liquid CO_2 on the density of the hydrate composite were investigated. It was hypothesized that increasing mass transfer at the water−liquid CO_2 interface in the reaction zone is the key to promoting hydrate production. A reactor model was formulated to explain the observed relationship between hydrate composite density and flow rates of CO_2 and water in the coflow reactor. Incorporating the laboratory physical and chemical data into a plume model, we simulated the sinking behavior of the CO_2 hydrate composite in the ocean. The results of this simulation are compared with simulation of pure hydrate and pure liquid CO_2 plumes.

Experimental Arrangement and Methods

A schematic diagram of the experimental system is shown in Figure 1. The test section of the system was placed in a large pressurized vessel, the Seafloor Process Simulator (SPS),

* Corresponding author phone: (865)241-3246; e-mail: tsourisc@ornl.gov.
[†] Oak Ridge National Laboratory.
[‡] University of Wales.
[§] Massachusetts Institute of Technology.

10.1021/es026301l CCC: $25.00 © 2003 American Chemical Society
Published on Web 07/18/2003

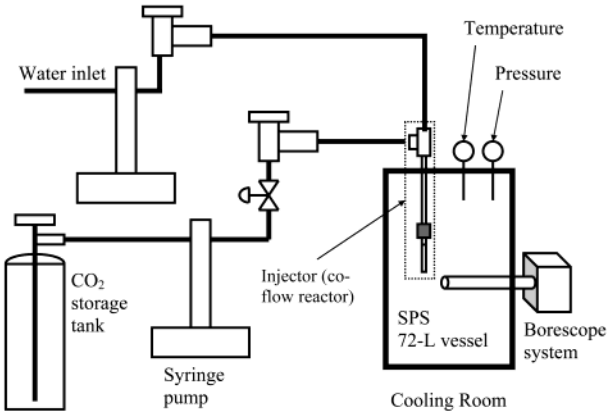

FIGURE 1. Experimental arrangement for producing CO_2 hydrate composite (not to scale).

which has been described in detail elsewhere (*22*, *23*). Briefly, the vessel is made of Hastelloy C-22 to resist seawater corrosion and has an internal diameter and length of 31.75 and 91.44 cm, respectively, providing a reaction volume of 72 L. It is equipped with sapphire windows, sampling ports, and measuring devices such as thermocouples (Hastelloy-sheathed type K thermocouples, with an accuracy of ±0.2 °C; ARI Industries, Inc., Addison, IL), pressure transducers, and pH probes. The SPS is capable of maintaining a pressure up to 20 MPa, and the pressure is controlled by compressed gas using a gas booster connected to the top of the vessel. Thermocouples were placed in both the gas and the liquid phases. Temperature and pressure data were collected periodically in 10−30-s time intervals using a data acquisition system consisting of National Instruments FieldPoint modules connected to a computer. Fluid delivery and recovery systems as well as backpressure regulators (Tescom, model 26-1724-24) attached to the top of the vessel allowed fluid flow while maintaining constant pressurization.

The test section was a coflow injector consisting of an outer tube (9.5 mm o.d. and 6.4 mm i.d.) and an inner capillary tube (1.6 mm o.d. and 125 μm i.d.) (Figure 2). The internal diameter of the capillary is important for producing the sinking CO_2 hydrate composite (see Modeling section). The stainless steel capillary tube terminates approximately 125 mm from the end of the outer tube, which consists primarily of stainless steel with a 140-mm section of Teflon at the end to prevent wetting of the wall by water in the mixing zone and to keep the water dispersed (Figure 2). Liquid CO_2 and water were pumped through the outer and inner capillary tubes, respectively, with two syringe pumps (ISCO model 100DM) at constant flow rates. The coflow injector can be placed horizontally (through the side port) or vertically (through the top port) in the SPS. The vertical orientation is shown in Figure 1. All equipment was kept in a temperature-controlled cold room.

In a typical experiment, the SPS was filled with approximately 60 L of doubly deionized distilled water at ambient conditions (1 atm, 25 °C). It then was transferred to the ~4 °C cold room and pressurized with nitrogen gas up to the experimental pressure (10.3−13 MPa). The system pressure was held constant until the internal vessel temperature reached 4 °C ± 0.8. Water (100 mL) and liquid CO_2 (60 mL) loaded in the syringe pumps were also placed in the cold room to allow them to reach the experimental temperature. After the entire system was stabilized with respect to temperature, the injection experiment began with the pumping of liquid CO_2 into the reactor at a constant volumetric flow rate. This injection continued until large CO_2 droplets were observed exiting the end of the Teflon section

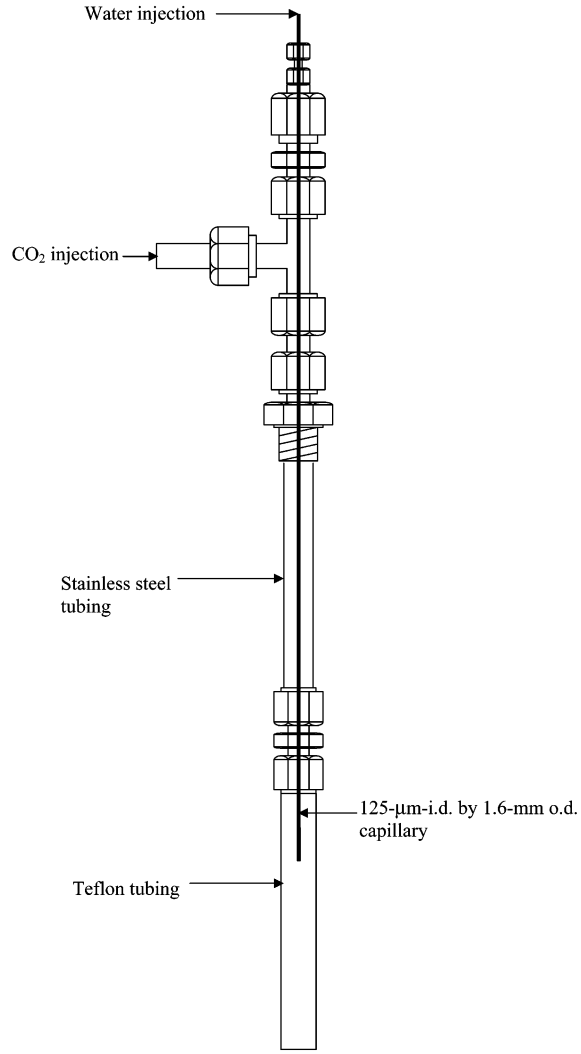

FIGURE 2. Coflow reactor used to form hydrate composite.

of the reactor (Figure 2). Water was then injected at the desired flow rate into the liquid CO_2 through the capillary while CO_2 injection continued. During injection, the pressure in the SPS was held constant. Only small changes occurred in the monitored temperature because of the large thermal mass of the SPS that was kept at temperatures of 4−5 °C in the cold room. The formation of hydrate composite was controlled by varying the pressure and flow rates of water and liquid CO_2. The resultant hydrate composite at the end of the coflow injector was visually observed through an optical sapphire window and recorded by a Sony CCD-TR716 video camera for analysis. A borescope system was also used for visual measurements of the composite. This system consists of an 8 mm in diameter by 56 cm in length borescope with internal fiber-optic lighting system and a high-resolution Watec model 12370 (480-line resolution) color digital camera with a maximum shutter speed of 1/10 000 s. Other digital cameras, such as the Nikon COOLPIX 990, were also used. During injection, images were recorded at a rate of 60/s for further analysis.

Results and Discussion

All experiments were conducted using the same configuration of the coflow reactor. The residence time in the reactor was between 8 and 14 s, depending on the total water and CO_2 injection rates. However, different results were observed depending on whether the water was injected from the

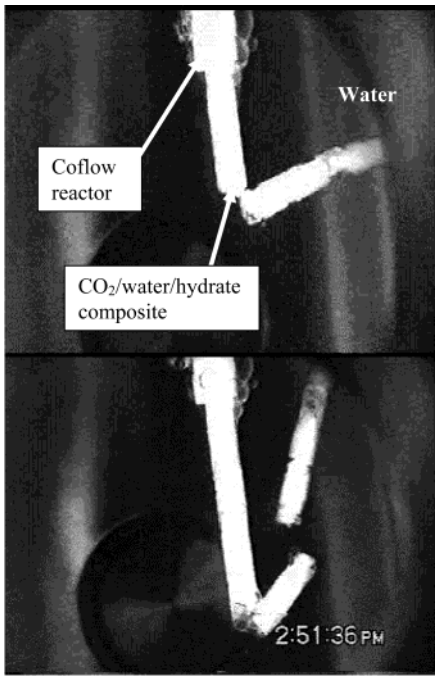

FIGURE 3. Sequential photographs of positively buoyant hydrate composite. $P = 10.5$ MPa; $T = 4.6$ °C; flow rates: $H_2O = 21$ mL min^{-1}, $CO_2 = 5$ mL min^{-1}.

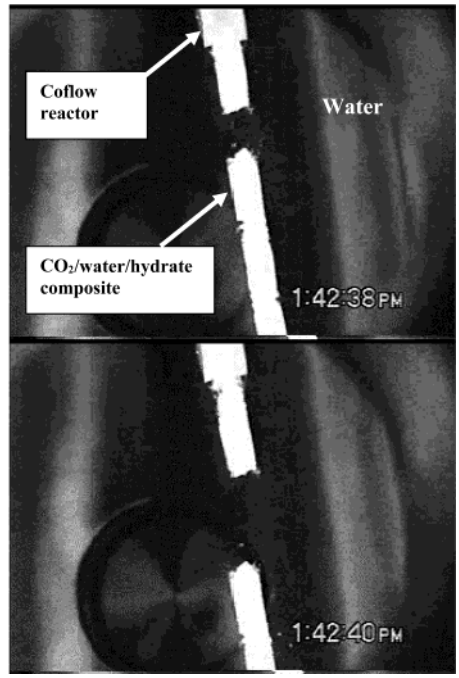

FIGURE 4. Sequential photographs of negatively buoyant hydrate composite. $P = 13.2$ MPa; $T = 4.1$ °C; flow rates: $H_2O = 23$ mL min^{-1}, $CO_2 = 6$ mL min^{-1}.

capillary into liquid CO_2 or vice versa. Earlier experiments showed that injection of liquid CO_2 alone produced rising droplets of liquid CO_2 that eventually became covered by a thin shell of CO_2 hydrate (*23*). However, injection of liquid CO_2 through the capillary into a continuous water phase produced clogging problems, as observed by others (*24*). When water was injected into liquid CO_2, a paste-like hydrate composite was produced at a temperature of ~4 °C and pressures of 10.3−13 MPa. Figures 3 and 4 show the paste-like hydrate composites that were discharged as a coherent cylindrical mass ~6 mm in diameter and ~5−10 cm long. Closer observation with a borescope showed hydrate-covered water droplets of uniform size "fused" together (Figure 5). Because water and liquid CO_2 are immiscible, injection of water into liquid CO_2 is hydrodynamically unstable: the water jet breaks up into droplets because of interfacial tension or hydrodynamic forces (*25*). Droplet generation is followed by rapid hydrate formation (*4, 26*) on the surface of water droplets because of subcooling conditions (about 6−7 °C subcooled below the temperature of CO_2−water−hydrate three-phase equilibrium). The hydrate layer prevented the water droplets from coalescing. Unlike the results of a previous study, in which the injection of liquid CO_2 into water (with jet velocities >15 cm s^{-1} and an orifice diameter <3 mm) produced "snow-like" structures in the droplet cloud (*27*), coherent hydrate composite masses were produced in this study. Because of the high volume fraction of the droplet phase in the restricted mixing zone, the droplets are very close to one another in the reactor resulting in aggregation of the hydrate-encased water droplets due to hydrogen bonding (*21*).

Sinking Characteristics of the Composite. The density of the hydrate composite could not be determined directly in the experimental system used in this work. Instead, the relative density of the composite with respect to the surrounding water was determined by visually observing whether the composite sank or floated. For the coherent mass formed in the coflow reactor (Figures 3 and 4), the buoyancy of the composite depends on the relative densities of the unconverted liquid CO_2, the water and the hydrate (*13*). Thus, the conversion of liquid CO_2 to hydrate determines whether the composite will sink or float. The density of the hydrate composite, ρ_{com}, is given by

$$\rho_{com} = \frac{44n_c + 18n_w}{44n_c(1/\rho_c - x_h(1/\rho_c - 1/\rho_h)) - 18(nx_h n_c(1/\rho_w - 1/\rho_h) - n_w/\rho_w)} \quad (1)$$

where ρ_c, ρ_w, and ρ_h are the densities of the liquid CO_2, water, and CO_2 hydrate, respectively; n_c and n_w are the initial numbers of moles of liquid CO_2 and water present, respectively; n is the hydration number; and x_h is the mole fraction of liquid CO_2 converted to hydrate. As used in this calculation, the molecular weights of CO_2 and water are 44 and 18, respectively. At a given mole fraction conversion (x_h), the density of the hydrate composite increases with ρ_c (eq 1), which increases with pressure because liquid CO_2 is compressible. Solving the equation for $\rho_{com}/\rho_w = 1$ yields a minimum mole fraction conversion (x_{h_min}):

$$x_{h_min} = \frac{1/\rho_c - 1/\rho_w}{(1/\rho_c - 1/\rho_h) + 18n(1/\rho_w - 1/\rho_h)/44} \quad (2)$$

When this threshold is exceeded, the hydrate composite will have a density greater than that of the ambient water. At a given T and P, this minimum conversion depends only on the hydration number and relative densities of liquid CO_2, hydrate, and water. Note, however, that x_{h_min} decreases with pressure largely because the density of liquid CO_2 increases considerably with pressure while the densities of water and hydrate are basically unchanged (*23, 28, 29*). For example, at 13 MPa (equivalent to 1.3 km depth) and 4 °C, eq 2 yields $x_{h_min} \approx 0.145$. To produce a sinking hydrate composite, one must convert enough liquid CO_2 to hydrate to exceed the mole fraction of 0.145. Experimentally, the hydrate mole fraction in the product was inferred to be greater or less than the threshold based on observations of whether the composite sank or floated. This inferred hydrate conversion was

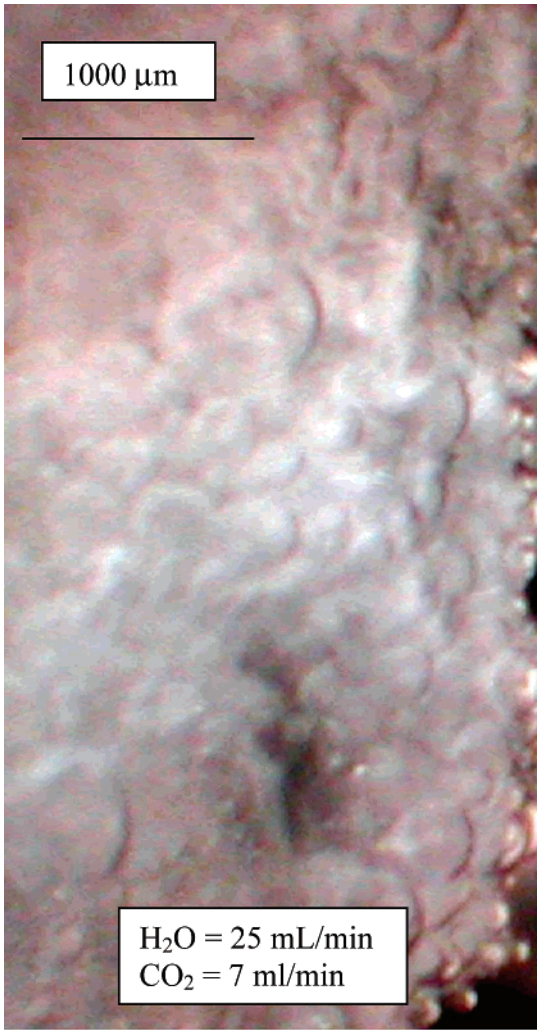

FIGURE 5. Surface of the hydrate composite as observed through a borescope, showing the small hydrate particles fused together.

observed to vary with mixing intensity, which depends highly on the rate of water injection.

Several sets of injection experiments were conducted at 10.3, 11.7, and 13.1 MPa, all at ~4 °C. Depending on the pressure, temperature, and flow rate conditions, the hydrate composite may be positively buoyant (Figure 3) or negatively buoyant (Figure 4). The main differences in the experimental conditions used in Figures 3 and 4 are the flow rates of water and CO_2 and pressure. The density of the composite was observed to increase with increasing pressure. Table 1 shows the maximum measured CO_2 flow rate that produced a negatively buoyant hydrate composite. When the maximum CO_2 flow rate is exceeded (e.g., 5 mL min^{-1} as compared with the maximum value of 3.5 mL min^{-1} in run 1.1 of Table 1), a positively buoyant composite is obtained (Figure 3). With a CO_2 flow rate equal to or lower than the maximum (e.g., 6 mL min^{-1} as compared with the maximum value of 7.5 mL min^{-1} in run 3.4 of Table 1), a negatively buoyant composite is produced (Figure 4). Quantitative experimental data separating the "positively buoyant" and "negatively buoyant" regimes are shown in Figure 6. The positively buoyant regime corresponds to the region above the line for the thermodynamic conditions represented by each line, while the negatively buoyant regime falls below the line. For instance, if the initial flow conditions fall in the positively buoyant regime (point A in Figure 6), one can decrease the CO_2 flow rate (point B) or increase the water flow rate (point C) to switch to the negative buoyancy regime, provided that the other conditions remained unchanged. When the operating conditions are changed from point A to point B or point C, at the point at which they coincide with the line, the hydrate composite becomes denser than the surrounding water. The minimum conversion of CO_2 required to produce a denser composite has been shown to be intrinsic to pressure and temperature and independent of the water and CO_2 flow rate (eq 2). However, it was determined experimentally that at a given CO_2 flow rate there is a minimum water injection rate that is necessary to make a denser composite product. This observation suggests that the water flow rate affects mixing and mass transport rates, which control the actual conversion rate.

TABLE 1. Experimental Conditions for Producing a Sinking CO_2 Hydrate Composite[a]

expt run	P (MPa)	T (°C)	water flow rate (mL min^{-1})	N_{Re} in capillary	N_{Re} of water droplets[b]	max liquid CO_2 flow rate (mL min^{-1})
1.1	10.5	4.2	21	2491	2.37	3.5
1.2	10.4	4.2	22	2609	2.51	4
1.3	10.4	4.8	23	2728	2.61	4
1.4	10.4	4.6	24	2846	2.80	5
1.5	10.5	4.5	25	2965	3.00	6
2.1	11.8	4.1	20	2372	2.22	3
2.2	11.8	4.4	21	2491	2.46	4.5
2.3	11.8	4.1	22	2609	2.71	6
2.4	11.8	4.6	23	2728	2.90	7
2.5	11.9	4.3	24	2846	2.95	6.5
2.6	11.8	4.5	25	2965	3.09	7
3.1	13.2	3.9	19	2253	2.22	4
3.2	13.1	4.5	20	2372	2.51	6
3.3	13.2	4.4	22	2609	2.80	7
3.4	13.2	4.2	23	2728	2.95	7.5
3.5	13.2	5.1	24	2846	3.09	8
3.6	13.2	4.4	25	2965	3.24	8.5

[a] For each experiment set, the maximum liquid CO_2 flow rate is determined. Rising hydrate composite was produced when the liquid CO_2 flow rate exceeded the maximum. [b] The measured droplet size (267 μm) is used for the N_{Re} calculations.

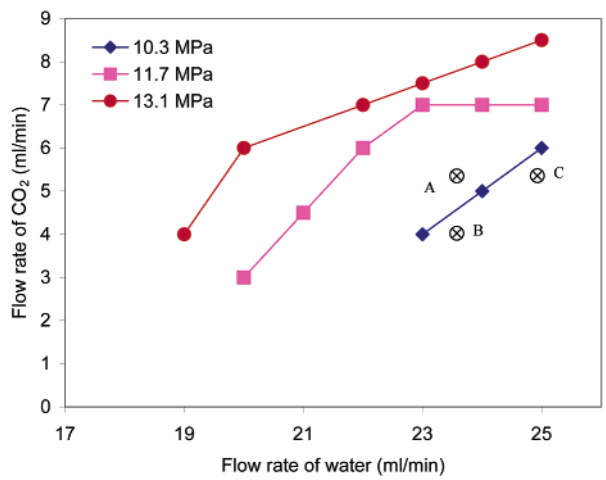

FIGURE 6. Density boundaries for producing a negatively buoyant hydrate composite. Point A denotes flow conditions for a positively buoyant hydrate composite at 10.3 MPa. Decreasing the CO_2 flow rate (to reach point B) or increasing the water flow rate (to reach point C) produces a sinking hydrate composite.

Gas Hydrate Formation Mechanism. Gas hydrate formation in the reactor appears to follow two consecutive steps: (i) water droplet formation and (ii) gas hydrate formation on the surface of the water droplets. Because gas hydrate formation occurs at the interface between liquid CO_2

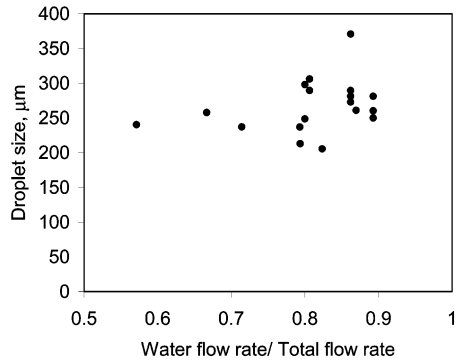

FIGURE 7. Water droplet size as a function of the ratio of water flow to total flow rate.

and water, the reaction rate is proportional to the surface area (i.e., the total surface area of water droplets) (*30*). For the estimation of the total surface area available for the reaction, the water droplet size distribution was measured with the borescope system described in the previous section. In Figure 7, the average droplet size is plotted as a function of the ratio of water flow rate to the total flow rate; this ratio represents the volume fraction of the droplet phase. No systematic change was noted in the average size of the water droplets with the changes in the volume fraction of the dispersed phase for the range of conditions used in the experiments. Significant fluctuations in the droplet size were observed as the volume fraction of the dispersed phase was increased. However, as a first approximation, the water droplet size was assumed to be constant, regardless of the flow rate of water and CO_2. The average drop diameter, obtained using the borescope system, was found to be 267 μm with a standard deviation of 79 μm.

The water drop size can also be calculated by using Weber's instability theory. According to this theory, the droplet size is independent of the velocity of water flow rate through the nozzle. The following equation is derived for calculating the water droplet size at the end of the water jet (*25*):

$$\frac{r}{r_j} = \left(\frac{3\pi}{\sqrt{2}}\right)^{1/3}(1 + 3Z^*)^{1/6} \tag{3}$$

where $Z^* \equiv (3\mu_D + \mu_c)/(d_o\sigma\rho)^{1/2}$; μ_D and μ_C are the viscosities of dispersed water and continuous liquid CO_2 phases, respectively; r is the radius of the droplet; and r_j is the radius of the jet, which is approximated by $1.88r_c$ (*25*). Here, r_c is the internal diameter of the capillary and d_0 is the opening of the orifice, which is $\sim 2r_c$. Using eq 3, we calculated the droplet diameter for the conditions of the experiments as 310 μm. This value compares favorably with the experimental value of 267 ± 79 μm that was obtained from the measurements.

The production of CO_2 hydrate on the surface of water droplets is derived by the steady-state hydrate conversion (x_h) in the coflow reactor at the experimental pressure and temperature, which is defined as follows:

$$x_h = \frac{\text{total moles of hydrate formed, } M_h}{\text{total moles of } CO_2 \text{ injected, } M_c} = \frac{M_h}{Q_c\rho_c/44} \tag{4}$$

where Q_c is the CO_2 flow rate and M_h and M_c are expressed as moles per unit time. The total number of moles of hydrate was calculated based on the amount of hydrate formed on a single water droplet (M_{h_drop}) surrounded by liquid CO_2 and the number of water droplets (N_{drop}) introduced in the reactor per unit time:

$$M_h = N_{drop}M_{h_drop} = \frac{Q_w}{\frac{4}{3}\pi r^3}M_{h_drop} \tag{5}$$

where r *is* the radius of water droplet and Q_w is the water flow rate.

Mass Transfer-Limited Model. The growth of hydrate films (related to the amount of hydrate formed) at interfaces between liquid CO_2 and water has been widely studied (ref *31* and references therein). Because hydrate formation and decomposition at fluid interfaces are not completely understood, different models for predicting hydrate film thickness have been and continue to be proposed (*32*). In the absence of specific parameters needed for the models described by Mori (*32*), we calculate the hydrate film thickness on a water droplet by assuming that diffusion of CO_2 molecules into the water phase controls hydrate formation, analogous to mass transfer on a CO_2 droplet (*31*, *33*). The change in the hydrate thickness on a CO_2 droplet results from hydrate growth and dissolution, which are controlled by mass transfer from liquid CO_2 into water depending on the saturation state of CO_2 in water (*20*, *31*, *34*). For the case in which a liquid CO_2 droplet is surrounded by water, a mass transfer model has shown that the hydrate shell greatly reduces the mass transfer of CO_2 into water (*19*, *28*, *35*). The rate of change of the hydrate shell is limited by mass transfer, expressed as $dr/dt = k^*$, where r is the radius of the drop and k^* is the overall mass transfer coefficient (*19*). The value of k^* is estimated to be between 10^{-7} and 10^{-6} m s^{-1} in the presence of a hydrate shell (*19*, *28*, *34*).

Using a similar approach to that shown in Ogasawara et al. (*19*), we calculate the amount of hydrate formed on the surface of a water droplet with an initial radius of r_0 as follows:

$$M_{h_drop} = \frac{4\pi}{3}[(\Delta r + r_0)^3 - r_0^3]\frac{\rho_h}{MW_h} \tag{6}$$

$$\Delta r = \int_0^{\Delta t} k^* \, dt \tag{7}$$

where MW_h is the molecular weight of the hydrate, Δr is the thickness of the hydrate shell, and Δt is the residence time in the reactor. Equation 7 is similarly derived as eq 2b in Ogasawara et al. (*19*), with a water drop replacing the liquid CO_2 drop. Accordingly, k^* is the overall mass transfer coefficient across the hydrate film. Combining eqs 4−6, one derives

$$x_h = \frac{44\rho_h}{MW_h\rho_c}\frac{Q_w}{Q_c}\left[\left(\frac{\Delta r}{r_0} + 1\right)^3 - 1\right] \tag{8}$$

or

$$x_h = \frac{44\rho_h}{MW_h\rho_c}\frac{Q_w}{Q_c}\frac{3\Delta r}{r_0} \tag{9}$$

The latter expression (eq 9) is obtained because the thickness of the hydrate shell, Δr, is normally on the order of 1−10 μm (*31*, *34*, *35*), making $\Delta r/r_0 < 1/20$.

At constant temperature and pressure, hydrate conversion will increase with an increasing ratio of water to CO_2 flow rate (Q_w/Q_c) and will decrease with increasing water droplet size (r_0) (eq 9). Additionally, because the thickness of hydrate layer (Δr) is a function of the mass transfer rate (eq 7), the hydrate conversion implicitly depends on mixing intensity as expressed by the Reynolds number, N_{Re}. In the absence of hydrate, the mass transfer coefficient was demonstrated to increase from 1 to 10 μm s^{-1} with increasing values of N_{Re} from 10 to ~2000, while in the presence of hydrate, the mass

TABLE 2. Hydrate Conversion Calculated with Equation 5, Based on a Mass Transfer-Limited Model[a]

Flow rate of water (mL min^{-1})	Flow rate of liquid CO_2 (mL min^{-1}) 2.5	3	3.5	4	4.5	5	5.5	6	7
19	[b]	**0.186**	**0.158**	0.136	0.120	0.107	0.096	0.08	0.074
20	[b]	**0.193**	**0.164**	0.142	0.125	0.111	0.100	0.091	0.077
21	[b]	**0.200**	**0.170**	**0.147**	0.130	0.116	0.104	0.095	0.080
22	[b]	**0.207**	**0.176**	**0.153**	0.135	0.120	0.108	0.099	0.083
23	[b]	**0.215**	**0.182**	**0.158**	0.140	0.125	0.112	0.102	0.086
24	[b]	**0.222**	**0.189**	**0.164**	**0.145**	0.129	0.116	0.106	0.090
25	[b]	**0.229**	**0.195**	**0.169**	**0.149**	0.133	0.120	0.110	0.093

[a] Expressed as the ratio of moles of hydrate to the initial moles of injected liquid CO_2. Calculation is made for a coflow reactor with 125 μm capillary, 6.4 mm diameter by 140 mm length of mixing zone at 10.3 MPa and 4 °C. Water droplet size is 267 μm. The bold numbers represent values greater than the minimum conversion under the *P* and *T* conditions ($x_{h_min} = 0.145$) as calculated by using eq 2. Flow conditions under which sinking composites were experimentally obtained are shown below the horizontal broken lines. [b] No hydrate formation.

transfer coefficient increased from 0.3 to 2 μm s^{-1} with increasing N_{Re} (*19*). Fitting data from Figure 4 in Ogasawara et al. (*19*), the overall mass transfer coefficients (in m s^{-1}) without hydrate (k_{l-l}) and with hydrate (k_{l-h}) are as follows:

$$k_{l-l} = 2.58 \times 10^{-7} + 6.26 \times 10^{-7}\, N_{Re}^{1/3} \qquad (10)$$

$$k_{l-h} = 0.23 \times 10^{-7} + 1.48 \times 10^{-7}\, N_{Re}^{1/3} \qquad (11)$$

In the coflow reactor used in this work, the value of N_{Re} varied from 2200 to 3000 in the capillary to 2.2−3.3 for water droplets in the mixing zone (see Table 1). Because of the complexity of the system, for the calculation of Δr, the following approximations have been made:

(i) At times <0.2 s, mixing is characterized by the capillary N_{Re}, and mass transfer is characterized by the overall mass transfer coefficient (k_{l-l}) without a hydrate shell.

(ii) At times >0.2 s, mixing is characterized by the N_{Re} of the water droplets, and mass transfer is represented by the overall rate with hydrate present.

These assumptions are considered reasonable because the jet breakup time is reported as ~0.2 s (*25*). The water droplets did not coalesce following the jet breakup, indicating that hydrate has begun to form on the droplets. The thickness of the hydrate shell, as expressed in eq 7 is then calculated by

$$\Delta r = 0.2 k_{l-l} + (\Delta t - 0.2) k_{l-h} \qquad (12)$$

The residence time is determined by the reactor size (6.4 mm diameter by 140 mm length) and the total flow rates of water and CO_2. Substituting eq 12 into eq 8, we calculated the hydrate conversion at 4 °C and 10.3 MPa as a function of the relative flow rate of water and CO_2 (Table 2).

Limits of Flow Rate Ratio. As Table 2 indicates, both increasing the water flow rate and decreasing the CO_2 flow rate have the effect of increasing hydrate conversion and producing sinking hydrate composite. However, a critical value of Q_c/Q_w exists. As determined in a previous study, the CO_2 mole fraction in aqueous solution must reach a critical value (Y_{CO_2} = 0.034−0.036) for hydrate formation (*3*). By converting this value to the flow rates used here, it was found that Q_c/Q_w must be >0.1. For the maximum water flow rate used in Table 2, hydrate formation should not be expected at CO_2 flow rates <2.5 mL min^{-1}, and in fact, hydrate formation was not observed under these conditions.

In general, Table 2 shows good agreement between experimental data and modeling results, where the flow conditions under which sinking CO_2 hydrate composite was observed (below broken line), matched well with those corresponding to the bold numbers. The bold numbers of Table 2 are greater than the minimum hydrate conversion ($x_{h_min} \sim 0.145$) as calculated by eq 2. At a given set of pressure and temperature values, the model predicted an increasing hydrate conversion with increasing water flow rate (columns 4−7 of Table 2). Experiments have shown that increasing water flow rate generally results in a buoyancy reversal from positive to negative at a fixed liquid CO_2 flow rate. The effect of water flow on hydrate formation may result from a combination of an increased reaction area and increased mixing energy. At steady state, the total reaction surface area can be shown to be proportional to Q_w/r_0. Thus, both increasing the water flow rate and reducing the size of water droplets (e.g., by using a smaller capillary orifice; see eq 3) would increase the reaction area, which is a key factor in increasing hydrate production.

Increasing the water flow rate also results in increased Reynolds number, which has the effect of enhancing the mass transfer rate between water and CO_2, as demonstrated in dissolution experiments (*19*, *34*, *36*). Calculations using eqs 5 and 6 showed that mass transfer rates in liquid−liquid and hydrate−liquid phases were equally important for the total hydrate conversion. As the water flow rate increased from 19 to 25 mL min^{-1}, the N_{Re} in the capillary increased proportionally (by 32%), resulting in a 9% increase in k_{l-l} (eq 10). The increase in the N_{Re} for water droplets in the mixing zone is slightly smaller (27%), but the effect on k_{l-h} is a 7.4% increase (eq 11). The effect from the increases in mass transfer coefficients (k_{l-l} and k_{l-h}) alone represents an increase in the hydrate conversion by 8%. If the effect of increased reaction surface area is included, a 23% increase in hydrate conversion is obtained.

Additionally, a flow rate increase will result in a decrease in the residence time in the reactor. Although not shown explicitly in Table 2, the residence time decreases with the CO_2 flow rate (from left to right in Table 2) and with water flow rate (from top to bottom in Table 2), respectively. Because the hydrate shell thickness is directly proportional to the residence time (eq 7), the hydrate conversion should be expected to increase with residence time. For example, a 25% increase in residence time (8−12 s) could increase the hydrate shell thickness from 3.3 to 4.2 μm when the other parameters are held constant at 4 °C and 10.3 MPa. However, because of the fixed reactor volume, increasing the residence time will necessarily decrease the total flow rate. Compared with the effect of increasing flow rate on hydrate conversion, the effect of reducing the residence time is small for the coflow reactor used in this work.

Some discrepancies exist between the model and experimental observations (Table 2). At high water and CO_2 flow rates, a sinking hydrate composite was obtained experimentally, despite the fact that the model predicted hydrate conversions $< x_{h_min}$ at the given pressure. Additionally, at relatively low water and CO_2 flow conditions, a sinking composite was not observed, although the model predicted a hydrate conversion higher than the minimum. The likely explanation for these discrepancies might be the uneven distribution of water droplet size, which causes inaccuracies in the prediction of the total reaction area. Although the water droplet size was considered independent of the flow velocity, the deviation in the average size of water drops for a particular run might affect the interaction area sufficiently and, hence, the hydrate production. Most importantly, lack of experimental data on CO_2 concentration in water and water in liquid CO_2 and corresponding solubility data limit our ability to use more sophisticated models as presented by Mori (*31*) on hydrate formation. For example, the initial estimate of thickness of hydrate films could have considered heat transfer (*37*) because hydrate formation raises the temperature at the reaction interface, promoting transport of CO_2 molecules (*28*) and significantly affecting further hydrate formation.

Additionally, the pressure effect is not explicitly considered in the model. As the pressure is raised, ρ_c is increased, which in turn reduces hydrate conversion (eq 9). However, the hydrate shell thickness (Δr) increases with pressure because of a greater driving force for hydrate formation at higher pressures (*38*). At a higher pressure, the minimum hydrate conversion also decreases (eq 2) (*23*). As a result, a higher pressure has the general effect of more easily producing a sinking hydrate composite. Experimentally, it was observed that increasing the pressure results in reversing the buoyancy of hydrate composites from positive to negative when flow rates and temperature are held constant. This effect is shown in Table 1, where for a CO_2 flow rate (Q_c) of 8 mL min^{-1}, the buoyancy of the hydrate composite is positive in run 2.6 [$Q_c >$ max Q_c (= 7 mL/min)] but negative in Run 3.6 [($Q_c <$ max Q_c (= 8.5 mL/min)] at a higher pressure.

Nevertheless we found that, within the limit of P and T conditions, eq 9, based on mass transfer-limited hydrate formation, shows the dependence of hydrate conversion on the water drop size and ratio of water to CO_2 flow rates. The most sensitive parameter affecting hydrate conversion is the radius of the water droplets, as shown in eq 9. The hydrate conversion would be reduced by 50% by raising the water droplet size 2-fold (from 300 to 600 μm) alone. This result is equivalent to enlarging the capillary internal diameter 2-fold from its initial size. Generally, a small capillary size produces small water droplets that have the same effect as producing very small CO_2 droplets in order to increase CO_2 hydrate conversion (*20*). Note that eq 9 may be used for the design of a laboratory reactor for further studies but should not be used for large-scale design. Current work is underway to study scale-up issues.

Seawater Experiments and Plume Modeling. Although this paper reported the results of using freshwater in the coflow reactor, experiments using saltwater were also conducted. Generally, greater hydrate conversion is needed to obtain sinking hydrate composite particles using seawater (data not shown). This is apparent from eq 2 where the density of seawater is greater than that of freshwater. Additionally, we performed experiments in the open sea and obtained hydrate conversion at ~0.25 (manuscript in preparation).

Because the individual composite particles produced both in the SPS and at sea were close to neutraly buoyant, they did not sink (or rise) very much, leading one to the initial conclusion that, without a greater hydrate conversion rate, injected CO_2 would not sink. However, in a real application where a stream of particles would be injected and their dissolution would drive a local increase in seawater density creating a negatively buoyant plume that would sink significantly. A dense single-phase plume discharged to a quiescent, stratified ambient seawater will sink and eventually become trapped by the ambient stratification at a depth h given by Turner (*39*) as approximately

$$h = \frac{2.8B_o^{0.25}}{N_{0.75}} \tag{13}$$

where B_o is the kinematic flux of (negative) buoyancy defined by $B_o = Q_o(\rho_o - \rho_a)/\rho_a)g$ and N is the stratification frequency given by $N = [g/\rho)(d\rho_a/dz)]^{0.5}$. Here Q_o is the initial volume flow rate of the plume, g is gravity, ρ_o and ρ_a are the initial plume and ambient densities, and z is depth. B_o can be related to the mass loading of CO_2 $\dot{m}_{CO_2}$ (in units of kg s^{-1}) as

$$B_o = \beta \dot{m} \tag{14}$$

where $\beta \cong 0.0019$ m^4 kg^{-1} s^{-2} (*7*, *40*).

In Table 3, we calculate the sinking depth h of a negatively buoyant plume formed from the instantaneous dissolution of neutrally buoyant composite particles injected into ambient waters characterized by $N = 0.003$ s^{-1}. Calculations are made for CO_2 mass injections of 1, 10, 100, and 1000 kg/s. Note that a 500-MW coal plant will produce a CO_2 stream of approximately 123 kg/s (*41*). The table also includes the corresponding average depths to which a plume of pure solid hydrates (i.e., 100% conversion efficiency) would sink before complete dissolution and the average heights to which a droplet plume of pure liquid CO_2 (i.e., 0% conversion efficiency) would rise (or, in the case of large loadings, the slight depth to which such a plume would sink). These additional calculations are made with an integral double-plume model assuming similar ambient conditions and an initial hydrate particle diameter of 1 cm (*42*) or an initial liquid droplet diameter of 0.5 cm (*43*). Clearly a conversion rate of order 25%, as reported herein, takes us a significant way toward maximum theoretical sinking (100% hydrate conversion). However, to use this method operationally, further studies should be conducted to address greater conversion efficiency, scale-up criteria, sequestration potential, and biological effects of dilute CO_2 plumes.

TABLE 3. Mean Sinking Depth (Rising Height) in Meters of CO_2 Plumes

hydrate conversion (%)	initial plume composition	CO_2 loading in kg/s: 1	10	100	1000
~25	composite particles	60	110	200	350
100	solid hydrate particles	250	400	700	1200
0	liquid CO_2 droplets	(30)	(30)	(70)	10

Acknowledgments

This research was supported by DOE Grant KP120203, Office of Science, Biological and Environmental Research, under Contract DE-AC05-00OR22725 with UT-Battelle, LLC. The authors are also thankful to Dr. J. Gabitto for fruitful discussions and to Dr. Marsha Savage for editing the manuscript.

Literature Cited

(1) U.S. Department of Energy, *Carbon Sequestration Research and Development*; Office of Science and Office of Fossil Energy: Washington, DC, December 1999.

(2) Golomb, D.; Zemba, S.; Dacey, J.; Michaels A. *Energy Convers. Manage.* **1992**, *33*, 675−683.
(3) North, W. J.; Blackwell, V. R.; Morgan, J. J. *Environ. Sci. Technol.* **1998**, *32*, 676−681.
(4) Brewer, P. G.; Friederich, G.; Peltzer, E. T.; Orr, F. M., Jr. *Science* **1999**, *284*, 943−945.
(5) Liro, C.; Adams, E.; Herzog, H. *Energy Convers. Manage.* **1992**, *33*, 667−674.
(6) Ozaki, M.; Sonoda, K.; Fujioka, Y.; Tsukamoto, O.; Komatsu, M. *Energy Convers. Manage.* **1995**, *36*, 475−478.
(7) Haugan, P.; Drange, H. *Nature* **1992**, *357*, 318−320.
(8) Nakashiki, N.; Ohsumi, T.; Shitashima, K. *CRIEPI Report EU 91003*; CRIEPA: Japan, 1991.
(9) Ohsumi, T. *Mar. Technol. Soc. J.* **1995**, *29*, 58−66.
(10) Sato K.; Sato T. *J. Mar. Sci. Technol.* **2001**, *6* (2), 59−69.
(11) Herzog, H. J. *4th International Conference on Green House Gas Control*; Switzerland, 1998.
(12) Alendal, G.; Drange, H. *J. Geophys. Res.* **2001**, *106* (C1), 1085−1096.
(13) Holder, G. D.; Cugini, A. V.; Warzinski, R. P. *Environ. Sci. Technol.* **1995**, *28*, 276−278.
(14) Hirai, S.; Tabe, Y.; Tanaka, G.; Okazaki, K. In *Greenhouse Gas Control Technologies;* Riemer, P., Eliasson, B., Wokaun, A., Eds; Elsevier Science: London, 1999; pp 317−322.
(15) Aya, I.; Yamane, K.; Shiozaki, K. In *Greenhouse Gas Control Technologies*; Riemer, P., Eliasson, B., Wokaun, A., Eds.; Elsevier Science: London, 1999.
(16) Rau, G. H.; Caldeira K. *Energy Convers. Manage.* **1999**, *4*, 1803−1813.
(17) Auerbach, D. I.; Caulfield, J. A.; Adams E. E.; Herzog, H. J. *Environ Model. Assess.* **1997**, 333−343.
(18) Teng, H.; Yamasaki, A.; Shindo, Y. *Energy* **1996**, *21*, 765−774.
(19) Ogasawara, K.; Yamasaki, A.; Teng, H. *Energy Fuels* **2001**, *15*, 147−150.
(20) Shindo, Y.; Sakaki, K.; Fujioka, Y. *Energy Convers. Manage.* **1996**, *37*, 485−489.
(21) Yamasaki, A.; Wakatsuki, M.; Teng, H.; Yanagisawa, Y.; Ymada, K. *Energy* **2000**, *25*, 85−96.
(22) Phelps, T. J.; Peters, D. J.; Marshall, S. L.; West, O. R.; Liang, L.; Blencoe, J. G.; Alexiades, V.; Jacobs, G. K.; Naney, M. T.; Heck, J. L., Jr. *Rev. Sci. Instrum.* **2001**, *72*, 1514−1521.
(23) West, O.; Tsouris, C.; Liang, L.; Lee, S.-Y.; McCallum, S. *AIChE J.* **2003**, *49*, 283−285.
(24) Morgan, J. J.; Blackwell, V.; Johnson, D. E.; Spencer, D. F.; North, W. J. *Environ. Sci. Technol.* **1999**, *33*, 1448−1452.
(25) Teng, H.; Kinoshita, C. M.; Masutani, S. M. *Int. J. Multiphase Flow* **1995**, *21*, 129−136.
(26) Sakai, H.; Gamo, T.; Kim, E.-S.; Tsutsumi, M.; Tanaka, T.; Ishibashi, J.; Wakita, H.; Yamanok M.; Oomori, T. *Science* **1990**, *248*, 1093−1096.
(27) Aya, I.; Yamane, K. *Proc. ASME Heat Transfer Div.* **1993**, *HTD-215*, 17−22.
(28) Teng, H.; Yamasaki. A. *Energy Convers. Manage.* **2000**, *41*, 929−937.
(29) Millero, F. J. *Geochimi. Cosmochem. Acta* **1995**, *59*, 661−677.
(30) Englezos, P.; Kalogerakis, N.; Dholabhai, D.; Bishnoi, P. R. *Chem. Eng. Sci.* **1987**, *42*, 2647−2658.
(31) Mori, Y. H. *Energy Convers. Manage.* **1998**, *39*, 1537−1557.
(32) Mori, Y. H. *Energy Convers. Manage.* **1998**, *39*, 369−373.
(33) Teng, H.; Kinoshita, C. M.; Masutani. S. M. *Chem. Eng. Sci.* **1995**, *50*, 559−564.
(34) Shindo, Y.; Fujioka, Y.; Takeuchi, K.; Komiyama, H. *Int. J. Chem. Kinet.* **1995**, *27*, 569−575.
(35) Uchida, T.; Kawabata, J. *Energy* **1997**, *22*, 357−361.
(36) Teng, H.; Yamasaki, A. *Heat Mass Transfer* **1998**, *41*, 4315−4325.
(37) Mori, Y. H. *J. Cryst. Growth* **2001**, *223*, 206−212.
(38) Malegaonkar, M. B.; Dholabhai, P. D.; Bishnoi, P. R. *Can. J. Chem. Eng.* **1997**, *75*, 1090−1099.
(39) Turner, J. S. *J. Fluid Mech.* **1986**, *173*, 431−471.
(40) Adams, E. E.; Golomb, D. S.; Zhang, X. Y.; Herzog, H. J. In *Direct Ocean Disposal of Carbon Dioxide*; Handa, N., Ohsumi, T., Eds.; Terra Scientific Publishers: Tokyo. 1995; pp 153−164.
(41) Herzog, H. J.; Golomb, D. S.; Zemba, S. *Environ. Prog.* **1991**, *10* (1), 64−74.
(42) Wannamaker, E. J. M.S. Thesis, Department of Civil and Environmental Engineering, MIT. Boston, MA, 2002.
(43) Crounse, B. C. M.S. Thesis, Department of Civil and Environmental Engineering, MIT. Boston, MA, 2000.

Received for review November 5, 2002. Revised manuscript received April 25, 2003. Accepted May 23, 2003.

ES026301L